Journal of Luminescence 181 (2017) 252–260

Contents lists available at ScienceDirect

Journal of Luminescence

journal homepage: www.elsevier.com/locate/jlumin

Full Length Article

Strong luminescence behavior of mono- and dimeric imidazoquinazolines: Swift OLED degradation under electrical current

Rampal Pandey [b,1], Gábor Méhes [c,1,2], Ashish Kumar [a], Roop Shikha Singh [a], Amit Kumar [a], Chihaya Adachi [c], Daya Shankar Pandey [a,*]

[a] Department of Chemistry, Institute of Science, Banaras Hindu University, Varanasi 221005, U.P., India
[b] Department of Chemistry, Dr. Harisingh Gour University, Sagar 470003, M.P., India
[c] Center for Organic Photonics and Electronics Research (OPERA), Kyushu University, 744 Motooka, Nishi, Fukuoka 819-0395, Japan

ARTICLE INFO

Article history:
Received 22 March 2016
Received in revised form
22 August 2016
Accepted 10 September 2016
Available online 15 September 2016

Keywords:
Imidazo-quinazoline
Crystal structure
Photoluminescence
Density functional theory
Excimer/ICT state formation
OLED degradation

ABSTRACT

Design and synthesis of novel mono- and dimeric quinazoline derivatives (+)-6-methyl-6-pyridin-2-yl-5,6-dihydrobenzo[4,5]imidazo[1,2-*c*]quinazoline (**1**) and (+)-6-[(6-methyl-5,6-dihydrobenzo-[4,5]imidazo[1,2-c]quinazolin-6-yl)-pyridin-2-yl]-6-methyl-5,6-dihydro-benzo-[4,5]imidazo-[1,2-*c*]quinazoline (**2**) have been described. Both **1** and **2** have been characterized by elemental analyses, FT-IR, ^{1}H and ^{13}C NMR, HRMS spectroscopic studies and their structures authenticated by X-ray single crystal analyses. Photophysical properties of these compounds have been studied by UV/VIS absorption and fluorescence spectroscopy and transient photoluminescence analysis in solution, powder, and non-doped (neat) and doped vacuum-deposited films. A broad emission spectrum spanning most of the visible range and good thermal stability indicated promising application of **1** and **2** as OLED emitters. Unfortunately, under current flow we observed rapid device degradation, presumably to be related to free –N*H* moiety in these compounds.

1. Introduction

Development of luminescent organic materials have fascinated the scientific community due to their unique electronic properties and potential application in photonics and optoelectronic devices *viz* solar cells [1–5], organic light emitting diodes (OLEDs) [6–9] and field-effect transistors etc. [2d] Usually, emission behavior of organic fluorophores in the solid state largely depends on entire molecule including intermolecular interactions controlling molecular packing rather than individual systems [10,11]. Interaction between monomeric chromophore and dimeric aggregates can radically change their photophysical properties [12–16]. In this context, molecular aggregates and multi-branched organic compounds exhibiting enhanced optical properties have drawn special attention. Consequently numerous dimeric systems have been designed and synthesized to compare their photophysical properties with respective monomeric counter-parts [12–24]. Though OLEDs have attracted enormous attention due to their wide applications in lighting and flat panel displays [6,7,25], their commercial applications are restricted owing to relatively poor electroluminescence (EL) stability especially those of blue emitting OLEDs for which EL efficiency decreases rather quickly during operation [26,27]. Usually, decrease of the intensity is coupled with the loss of blue color purity thus, realization of the cause of degradation for devices is highly demanding [28,29]. Furthermore, heterocyclic systems possessing quinoline and oxidiazole moieties display improved electron transport abilities [30,31] but due to poor luminescence these have scarcely been used as emitting layer in OLEDs [32–35].

With an intention of understanding the comparative photophysical properties of mono- and dimer, wherein conjugation for both of these are broken at the same position, two new systems with one (**1**) and two fluorophore arms (**2**) have been designed and synthesized. The crystallo-graphic, thermal, and theoretical studies illustrated close similarity between these imidazo-quinazolines which prompted us to compare their photophysical and electroluminescence properties. Resemblance in their photophysical properties arises due to the loss of planarity and conjugation at sp^3-hybridized carbon in both the systems (Fig. 1; *vide supra*). Further, these display high photoluminescence (PL) quantum yield (Φ_{PL}) along with an additional low energy (LE) emission band attributable

* Corresponding author.
E-mail address: dspbhu@bhu.ac.in (D.S. Pandey).
[1] Rampal Pandey and Gábor Méhes both have equal contributions
[2] Present address: Laboratory of Organic Electronics, Department of Science and Technology, Linköping University, SE-601 74 Norrköping, Sweden.

http://dx.doi.org/10.1016/j.jlumin.2016.09.026
0022-2313/

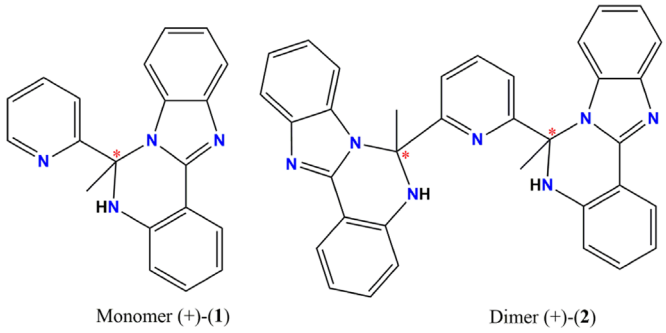

Fig. 1. Chemical structures of 1 and 2.

to dynamic emissive excimer or ICT states. The occurrence of two broad emission bands with almost equal intensity in non-doped neat films prompted us to examine suitability of these compounds as OLED emitters and to fabricate devices for white OLEDs (WOLEDs) [36,37]. Unfortunately, presence of the free –NH group in these systems lead to poor EL stability *via* swift OLED degradation for the devices as neat or doped film. Through this contribution we describe synthesis, characterization, comparative photophysical properties and OLED degradation behavior of **1** and **2**.

2. Experimental section

2.1. Materials

The solvents were dried and distilled following standard literature procedures [38]. 2-Acetyl-/2,6-diacetylpyridine and 2-aminophenylbenzimidazole were procured from commercial sources and used without further purifications.

2.2. General methods

C, H, and N analyses were performed on an Exeter Analytical Inc. Model CE-440 CHN analyzer. IR spectra were acquired on a Perkin-Elmer 577 spectrometer. ^{1}H (300 MHz) and ^{13}C (75.45 MHz) NMR spectra were obtained on a JEOL AL300 FT-NMR spectrometer using tetra-methylsilane [$Si(CH_3)_4$] as an internal reference. Non-doped (neat) and host-guest co-deposited films with **1** or **2** as the guest and 1,3-bis(9-carbazolyl)benzene(mCP) as host were fabricated on 01 mm thick quartz and 0.4 mm thick silicon substrates *via* high vacuum vapor deposition. The substrates were thoroughly cleaned with chloroform and acetone in an ultrasonic bath before deposition. During fabrication, vacuum pressure was maintained below 4.0×10^{-4} Pa and thickness of the organic films were 50–100 nm. Electronic absorption spectra were acquired on a Shimadzu UV-2550 and Perkin Elmer Lambda 950 spectrophotometers, while fluorescence on a JASCO FP-6500 and Horiba Fluoromax 4 Fluorescence Spectrophotometers. PL emission spectra and photoluminescence quantum yield on powdered samples were acquired on an absolute PL quantum yield spectrometer Hamamatsu C11347 Quantaurus QY equipped with an integrating sphere and xenon lamp for excitation through a monochromator. Transient PL characteristics were measured using Hamamatsu C11367-12 Quantaurus-Tau with embedded LED light source as excitation. The lifetimes τ_1, τ_2 for transient decays were determined using embedded software Quantaurus-Tau. Mass spectra for **1** and **2** in methanol were obtained on a JEOL-AccuTOF JMS-T100 LC mass spectrometer. Experimental highest occupied molecular orbital energy levels (HOMO) were determined using photoelectron yield spectroscopy on Riken Keiki AC-3, and lowest unoccupied molecular orbital energy levels (LUMO) calculated as HOMO – Eg, where Eg is energy gap determined from the onset of absorption spectra in neat films. OLEDs were fabricated on the top of glass substrates precoated with indium tin oxide (ITO, 110 nm). Substrates were thoroughly cleaned by washing with various organic solvents under ultrasonic treatment heated with an excess of isopropanol at 235 °C and by ozone and UV treatment prior to device fabrication. The fabrication method for EL study was same as for thin films. Current density–voltage–luminance (*J–V–L*) characteristics for OLEDs were measured using a semiconductor parameter analyzer Agilent E5270 with an optical power meter Newport 1930. EL spectra were obtained using spectrometer Ocean Optics USB2000. The CIE color coordinates were calculated using spectral EL intensity data and standard CIE color matching functions in the spectral range from 380 to 780 nm with 5 nm sampling. Optical rotation data were acquired on Autopol III polarimeter using 1 dm cell at 27 °C in DMSO as the solvent and concentration mentioned is g/100 mL.

2.3. X-ray structure determinations

Single crystal X-ray data for **1** and **2** were collected on a Bruker APEX II (kappa 4) diffractometer and for **M** on a OXFORD DIFFRACTION X CALIBUR-S at 25 °C using graphite monochromatized Mo-Kα radiation ($\lambda = 0.71073$ Å). Structures were solved by direct methods (SHELXS 97) and refined by full-matrix least squares on F^2 (SHELX 97) [39]. Non-hydrogen atoms were refined with anisotropic thermal parameters. Hydrogen atoms were geometrically fixed and refined using a riding model. Computer program PLATON was used for analyzing interaction and stacking distances [40]. CCDC deposition numbers 959911 (**1**), 959912 (**2**) and 959913 (**M**) contain supplementary crystallographic data for this paper.

2.4. Energy calculations

Following procedure was adopted for calculating energetic properties of the compounds under investigation. 2D Structures of the molecules were designed using Chem-BioDraw Ultra software, while 3D structures optimized using ChemBio3D Ultra by minimizing energy in *MM2* mode. Resulting structures were further optimized with Gaussian 09 by performing density functional theory (DFT) calculations in B3LYP mode using 6-31G(d) basis set in the ground state. These results were used to obtain HOMO and LUMO and electron density distributions on these levels. Energetic properties for **1** and **2** in excited state (singlet and triplet energy levels) were determined using Gaussian 09 with the same basis set but in time dependent mode (TD-DFT). To obtain singlet and triplet energy levels with greater precision number of states were set to 10.

2.5. Synthesis

Preparation of (+)-6-methyl-6-pyridin-2-yl-5,6-dihydrobenzo [4,5]imidazo[1,2-*c*]quinazoline (**1**). 2-Acetylpyridine (5.0 mmol) dissolved in ethanol (10 mL) was added to a stirring solution of 2-(2-aminophenyl)-1-benzimidazole (5.0 mmol) dissolved in the same solvent (20 mL) and reaction mixture heated under reflux for 6 h. Progress of the reaction was monitored by thin layer chromatography (TLC). After completion the reaction mixture was cooled to ambient temperature, concentrated to half its volume at reduced pressure and kept undisturbed in a refrigerator to afford microcrystalline compound. It was separated by filtration, washed with cold ethanol followed by diethyl ether and recrystallized from methanol. Yield (1.481 g, 94.9%): mp 225-230 °C; $[\alpha]_D$ + 2.32 (c 0.1, DMSO). Analytical data: Anal. Calc. for $C_{20}H_{16}N_4$ (312.14): C, 76.90; H, 5.16; N, 17.94. Found: C, 77.09; H, 4.99; N, 18.01. FT-IR (KBr; cm^{-1}): 3259 (m), 1613 (m), 1587 (s), 1509 (m), 1477 (s), 1443 (s), 1427 (m), 1309 (s), 1173 (m), 752 (vs), 732 (vs). ^{1}H NMR (DMSO-d_6, 300 MHz, δ_H, ppm): 8.57 (s, 1H), 7.90 (d, 1H); 7.83 (d, 1H), 7.63 (t, 1H); 7.45 (d, 1H); 7.34 (t, 1H); 7.36-7.15 (m, 2*H*); 7.07-

6.99 (m, 2H), 6.87-6.77 (m, 2H), 6.65 (t, 1H), 2.29 (s, 3H). ^{13}C NMR (DMSO-d_6, 75 MHz, δ_C, ppm): 150.12, 147.18, 146.73, 143.80, 142.68, 135.84, 133.33, 132.63, 131.81, 124.72, 123.98, 122.36, 118.71, 115.03, 112.01, 110.34, 28.86. HRMS (*m/z*) for $C_{20}H_{16}N_4$: [M^+] calcd 312.1375; found 312.2029.

Preparation of and (+)-6-[(6-methyl-5,6-dihydrobenzo-[4,5] imidazo[1,2-c]quinazolin-6-yl)-pyridin-2-yl]-6-methyl-5,6-dihydrobenzo-[4,5]imidazo-[1,2-*c*]quinazoline (**2**). It was prepared following the above procedure for **1** using 2,6-diacetyl-pyridine (2.5 mmol) and 2-(2-amino-phenyl)-1-benzimidazole (5.0 mmol) in 1:2 molar ratio. Yield (1.257 g, 92.1%): mp 218-220 °C; $[\alpha]_D$ + 6.17 (c 0.1, DMSO). Analytical data: Anal. Calc. for $C_{35}H_{27}N_7$ (545.23): C, 77.04; H, 4.99; N, 17.97. Found: C, 77.09; H, 4.99; N, 18.01. FT-IR (KBr; cm^{-1}): 3259 (m), 1612 (m), 1587 (m), 1539 (s), 1478 (s), 1375 (m), 1309 (m), 753 (vs), 733 (vs). ^{1}H NMR (DMSO-d_6, 300 MHz, δ_H, ppm): 7.88 [d (*br*), 2H]; 7.52-7.62 (m, 4H); 7.44 (s, 2H); 7.32-7.13 (m, 6H); 6.91–6.80 (m, 7H); 2.12 (s, 3H); 2.05 (s, 3H). ^{13}C NMR (DMSO-d_6, 75 MHz, δ_C, ppm): 159.87, 147.29, 142.87, 138.94, 133.23, 131.54, 124.64, 121.89, 120.22, 118.67, 114.42, 111.80, 25.72. HRMS (*m/z*) for $C_{35}H_{27}N_7$: [$M+H^+$] calcd 545.2328; found 546.2323.

Note: The chiral compounds **1** and **2** will most probably have their stereoisomers which were not separated as the present work is focused on photophysical behavior of these quinazoline systems. However, the optical rotation data showed (+)-form for both **1** and **2** which affirms chirality in these molecules. Therefore, reported yields concerned with the total yield of the product including stereoisomers.

Preparation of **M**: An aqueous solution (2 mL) of $FeCl_3 \cdot 6H_2O$ (0.269 g, 1.0 mmol) was added drop wise to a solution of **2** (0.545 g, 1.0 mmol) in methanol (10 mL) and resulting reaction mixture stirred for 10 min. A light green colored product quickly appeared which was filtered, washed thrice with water (3 × 5 mL) to remove free iron salt from the reaction mixture. Resulting greenish colored residue was recrystallized from methanol to afford **1′**. Yield (0.588 g, 90%). Analytical data: Anal. Calc. for $C_{35}H_{33}Cl_2N_7O_2$ (654.58); C, 64.22; H, 5.08; N, 14.98. Found: C, 64.28; H, 5.12; N, 15.04%. FT-IR (KBr; cm^{-1}): 3517 (s), 3426 (m), 3260 (s), 1627 (vs), 1568 (s), 1458 (m), 1385 (s), 1185 (s), 754 (vs), 741 (vs). ^{1}H NMR (DMSO-d_6, 300 MHz, δ_H, ppm): 8.20 [s (*br*) H-1, 2H, –*NH*] 8.02-7.96 (m, H-4, H-7, 4*H*); 7.79-7.70 (m, H-5, H-6, 4H); 7.38 (d, *J*=6.6 Hz, H-8, H-11, 4H); 7.08 [s (*br*), H-2, 2H]; 6.88 (m, H-3, H-9, H-10, 5H); 2.18 (s, H-12, 3H); 2.11 (s, H-12, 3H). ^{13}C NMR (DMSO-d_6, 75 MHz, δ_C, ppm): 158.01, 145.02, 143.67, 139.96, 135.28, 129.93, 125.39, 121.40, 118.62, 114.63, 112.94, 25.22. HRMS (*m/z*) for $C_{35}H_{33}Cl_2N_7O_2$: [M^+] calcd. 654.2106; found 654.1609.

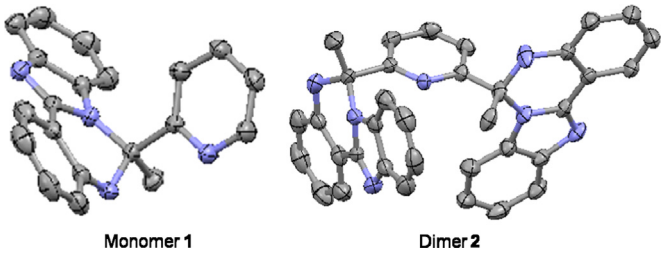

Fig. 2. Crystal structures of 1 (left) and 2 (right).

3. Results and discussion

3.1. Molecular design and synthesis

Designing of the systems for the present study involves incorporation of pyridyl ring as a core and one or two imidazoquinazoline (IQ) fluorophore arm(s). Syntheses of **1** and **2** have been achieved in reasonably good yield by condensation of 2-(2-aminophenyl)-1-benzimidazole with acetylpyridines. Simple strategy adopted for their synthesis is shown in Scheme S1 (SI) while molecular structures depicted in Fig. 1. These have been thoroughly characterized by satisfactory elemental analyses and spectral (IR, ^{1}H, ^{13}C NMR and mass) studies. Photophysical properties of a dimer may significantly differ relative to monomer provided that both fluorophore arms of the dimer are conjugated. Our prime concern to synthesize both **1** and **2** has been to examine the outcome of number of flurorophore units on photophysical properties of the systems if both the fluorophore units in dimer (**2**) are not conjugated. One can see from the chemical structures of **1** and **2** that these differ only in number of IQ units (one IQ in **1** and two IQ in **2**), however both the IQ fluorphores in **2** are not in conjugation with each other. It has been eventually unveiled by single crystal structural studies as well. A comparison of structures further revealed that extended conjugation between IQ arms is ruptured at sp^3-carbon centers in the dimer **2** (Fig. 1).

The presence of singlets (δ 7.04, **1**; 7.44 ppm, **2**) assignable to quinazoline –N*H* and methyl proton (2.29, **1;** δ 2.12 and 2.05 ppm, **2**) in the respective ^{1}H NMR spectra (Fig. S1 and S2, SI) strongly supported their formation. Information about –N*H* proton resonances in **1** and **2** has also been obtained by D_2O exchange since signal presumed to be associated with –N*H* proton overlapped with other signals. Molecular ion peak [M^+] at *m/z* 312.2029 (90%) for **1** and [$M+H^+$] at *m/z* 546.2323 (55%) for **2** (Fig. S5 and S6, SI) in the mass spectra and vibrations due to -N*H* (stretch) at 3259 (**1**) and 3260 cm^{-1} (**2**) also strongly suggested successful synthesis of **1** and **2**.

The optical rotation data showed average positive rotation {$[\alpha]_D$ = (+ve)} for both **1** and **2**. Notably, for **1** with one chiral center, both positive {$[\alpha]_D$ + 12.9, (c 0.1, DMSO)} and negative {$[\alpha]_D$ −3.4, (c 0.1, DMSO)} signs of the specific rotation with average value of $[\alpha]_D$ + 2.32 (c 0.1, DMSO) have been observed. On the other hand, **2** seems like a *meso*-chiral compound since one of its chiral centers shows 'R' configuration then other certainly in 'S' configuration (as chiral centers are anti disposed). Notably, the stereocenters are non-superimposable therefore, it is optically active and showed only positive specific rotations having $[\alpha]_D$ + 9.3 and +1.9 (c 0.1, DMSO) with an average positive specific rotation $[\alpha]_D$ + 6.17. The optical rotation data displayed average positive {$[\alpha]_D$ = (+ve)} specific

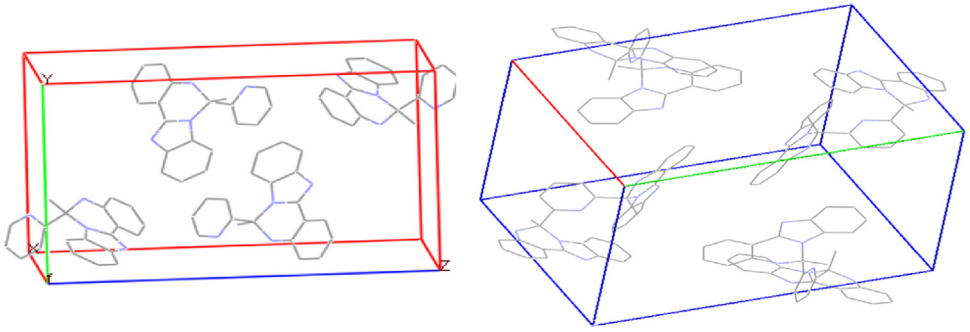

Fig. 3. Molecular packing in 1 (left) and 2 (right).

rotation for **1** but also indicated formation of (+) and (−) mixtures and therefore ruled out the formation of racemic mixture. Likewise, only positive specific rotations for **2** also overruled formation of the racemates. However, the absolute 'R' and 'S' configuration for **1** and **2** has not been assigned as the compounds were not separated. The separations although becomes essential provided that chiral molecules are probed toward asymmetric synthetic interest or chiral-to-chiral recognition etc.

3.2. Crystal structures

Both **1** and **2** crystallizes in monoclinic system with $P2_1/n$ space group. Perspective view of the compounds is given in Fig. 2, and important crystallographic parameters summarized in Table S1 (SI). The unit cell for both **1** and **2** contains four molecules (Fig. 3).

The members of IQ arm in **1** lies in and out of the IQ ring plane with deviations ranging from 0.045 to 0.270 Å (Fig. S7, SI) and almost planar with a deviation of 0.005 to 0.157 (first ring) and 0.004–0.176 Å (second ring) for **2**. Methyl group in **1** is disposed away from the central pyridyl ring plane while one of the methyl groups lies in pyridyl ring plane and other one out of the plane in **2** (Fig. S8, SI). The bite angles about sp^3 hybridized asymmetric carbon are close to ideal T_d geometry and fall in the range of 106.05–112.50° (**1**) and 107.56–113.76° (**2**). The plane containing central pyridyl ring in **1** bisects IQ arm keeping both quinazoline nitrogen [N(2) and N(3)] in the same face (Fig. S8, SI).

In contrary, central pyridyl ring plane passes exactly through middle of the quinazoline nitrogen in one of the IQ arms in **2** while bisects other IQ arm similar to that in **1**. It suggested that central pyridyl ring and one of the arms in **2** are oriented exactly in the same manner as in **1** and other IQ arm is oriented in a different manner. The C–C and C–N bond distances and angles are normal and fall in the range for analogous systems [41–43]. Structural studies on both **1** and **2** clearly suggested non planar structures for IQ arm(s) with respect to central pyridyl ring and rupture of conjugation at sp^3 hybridized asymmetric carbon which may be responsible for analogous photophysical behavior of **1** and **2**.

Usually, photophysical properties of the molecules especially in solid state are governed by non-covalent interactions (H···bonding, C–H···π, and π···π). Compound **1** involves inter-molecular hydrogen bonding between N(2)-H(21)···N(1) (3.062 Å) in a head-to-tail fashion and forms dimeric structure whereas inter-molecular H···bonding between N(2)-H(2)···N(4) (3.042 Å) leads to a linear infinite 1D chain in **2** (Fig. S9, SI). Notably, π···π interactions are lacking in both the compounds. It is worth mentioning that **1** involves ten C-H···π interactions (2.547–2.890 Å) while **2** only five (half to that for **1** and C–H···π interactions in the range of 2.796–2.899 Å, Fig. S10 and S11, SI). As far as supramolecular assemblies are concerned **1** involves sixteen short contacts with neighboring molecules leading to a football-like 3D supramolecular network (Fig. S12, left, SI). On the other hand, **2** involve ten short contacts creating a flower like 3D motif (Fig. S12, right, SI). Considering the structural features and greater extent of weak interactions **1** is expected to attain greater rigidity in the solid state thus superior photophysical properties relative to **2**. However, the existence of two IQ fluorophore units in **2** cannot be over-looked.

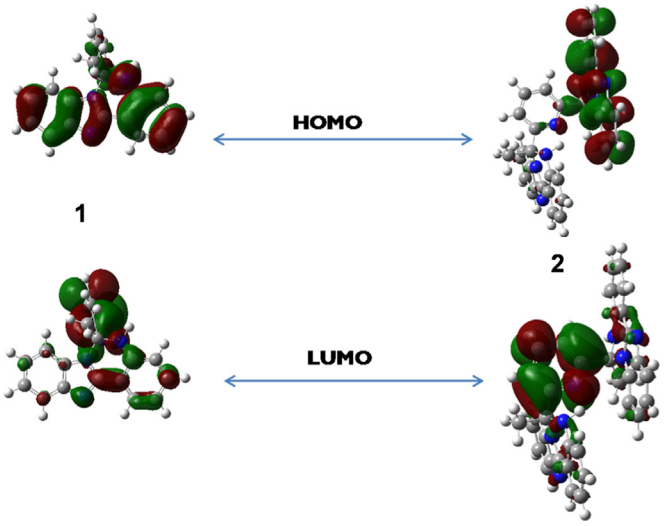

Fig. 4. Distribution of electron densities in HOMO and LUMO of 1 and 2.

3.3. Theoretical studies

One can predict the photophysical behavior of fluorophores by a comparison based on quantum-chemical calculations using Density Functional Theory (DFT). The calculations revealed that electron density on the HOMO of **1** is distributed mainly on the IQ arm (Fig. 4). On the other hand, despite presence of two IQ arms in **2**, electron density is distributed only on one arm. Electron density in LUMO for both **1** and **2** is chiefly distributed on pyridyl core. The energy envelope plots suggested a similar mechanism of electronic transitions in **1** and **2** [41].

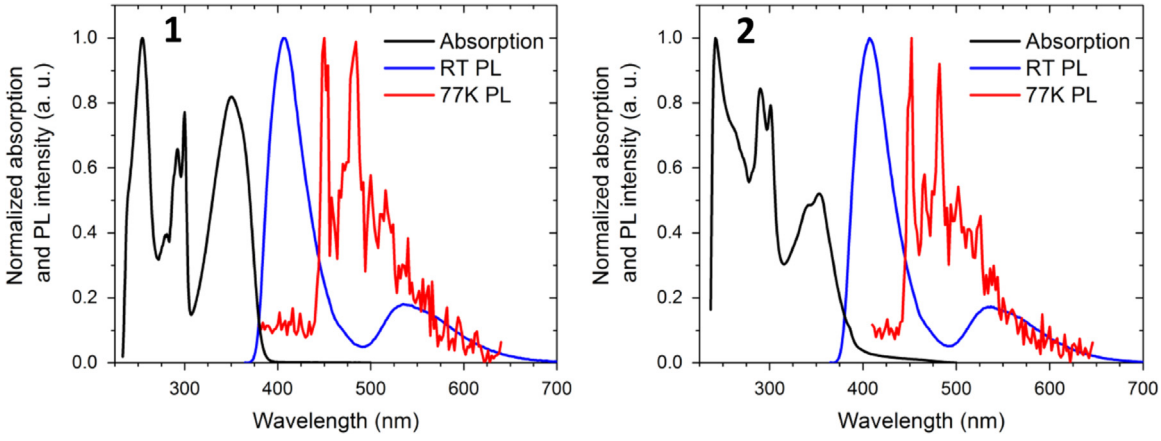

Fig. 5. Absorption at room temperature (RT, black line), emission at RT (blue line) and at 77K (red line) for 1 (left) and 2 (right) in 2-Me-THF at 10^{-5} M concentrations. (For interpretation of the references to color in this figure legend, the reader is referred to the web version of this article.)

Table 1
Photophysical parameters for **1** and **2**.

Medium	Emitter 1 2-Me-THF	Emitter 1 mCP	Emitter 1 Powder	Emitter 1 Neat film	Emitter 2 2-Me-THF	Emitter 2 mCP	Emitter 2 Powder	Emitter 2 Neat film
Φ_{PL} (%)	n/a	28.4	42.6	33.3	n/a	24.0	22.2	26.5
Absorption peaks (nm) [Extinction coefficient $\times 10^{-5}$($M^{-1}cm^{-1}$)]	255[4.4], 292[2.9], 300 [3.4], 350[3.6]	n/a	n/a	254, 291, 301, 323, 352	242[2.8], 290[2.4], 301[2.2], 342 [1.4], 353 [1.5]	n/a	n/a	255, 291, 301, 325, 352
PL emission peaks (nm)	406, 535	403, 543	410, 522	417, 521	407, 534	407, 537	415, 529	410, 528
Transient decay $\tau_{1,}\tau_2$ (ns) [Emission wavelength (nm)]	1.3 [407],9.9 [407]	2.2 [404],5.4 [404]	n/a	n/a	1.4 [407],5.0 [407]	2.0 [404],5.2 [404]	n/a	n/a

3.4. Photophysical properties

3.4.1. Absorption studies

UV/VIS spectra of **1** and **2** in diluted 2-Me-THF exhibited characteristic absorptions due to imidazo[1,2-*c*]quinazoline moiety (350, 300, 292 and 255 nm, **1;** 353, 342, 301, 290 and 242 nm, **2)** (Fig. 5 and Table 1) [41–43]. The low energy (LE) bands for **1** and **2** have been tentatively assigned to intramolecular charge transfer (ICT) and high energy (HE) ones to $\pi \rightarrow \pi^*$ transitions associated with IQ chromophore. To gain deep insight on $\pi \rightarrow \pi^*$ or ICT transition, the effect of solvents on absorption spectra of **1** and **2** has been investigated (Fig. S13b and Fig. S13c). Notably, in polar solvents the HE band exhibited small red shift ($\Delta\lambda$, 2–3 nm) whilst LE a significant red shift ($\Delta\lambda$, 15–20 nm). The position of absorption bands for **1** and **2** are comparable and suggested only a subtle effect of number of IQ units on their electronic transitions. In addition, absorption spectral features of **1** are alike to that of **2** in neat films, and resemble closely to those acquired in 2-Me-THF displaying peaks at ~352, 323, 301, 291, and 254 nm (Fig. S13a, SI). Less pronounced absorption bands at ~352 nm in neat films compared to those in solution can be attributed to molecular packing in the solid state. These results also suggested insignificant influence of the number of IQ units on their absorption behavior. UV/VIS spectral study indicated strong similarity between **1** and **2** in terms of electronic transitions. At the same time, significant change in absorption behavior of the low energy shoulder between diluted solution and neat films indicated substantial influence of the intermolecular interactions.

3.4.2. Emission studies

Due to presence of strong IQ fluorophore(s) both **1** and **2** are expected to show intense emission. Further, because of different number of IQ fluorophore units in these, it will be interesting to investigate relative emission behavior of **1** and **2.** Notably these displayed two emission bands in 2-Me-THF (10^{-5} M), strong photoluminescence (PL) [406 (**1**); 407 nm (**2**)] and low energy weak emissions [535 (**1**), 534 nm (**2**) (λ_{ex}, 350 nm)] (Fig. 5). All the experiments have been performed at room temperature unless otherwise stated. Separation between peaks of low and high energy bands is almost identical for **1** ($7.752 \times 10^4\ cm^{-1}$) and **2** ($7.874 \times 10^4\ cm^{-1}$). This dual emission in solution (strong HE and weak LE band) may be attributed to the dynamic existence of single molecule and excimers/ICT states via IQ fluorophore (*vide supra*). The dynamic emissive excimers or ICT state formation in 2-Me-THF has been further supported by loss of LE band in polar solvents like MeOH, DMF and DMSO and dual emission in 2-Me-THF, CH_2Cl_2 and CH_3CN (Fig. S14, SI). Further, emission behavior of **1** and **2** at 77K in 2-Me-THF (10 ms delay, 10^{-5} M) displayed a single emission characteristic of π–π* transitions with two vibronic peaks at λ_{max} 450 and 480 nm for **1** and **2** (Fig. 5).

The dual emission in solution (strong HE and weak LE band) may be ascribed to the presence of dynamic excimer or ICT states preferably occur in non-polar aprotic solvent like 2-me-THF (Fig. S14, Fig. S15). To have better insight into this phenomenon, we have examined the effect of solvent on **1** or **2** (Fig. S14) and observed that in solvents like MeOH, DMF and DMSO these exhibited single emission whereas dual emissions in 2-Me-THF, CH_2Cl_2 and CH_3CN wherein the LE band is weaker in intensity (Fig. S14). Intensity of the LE emission band follows the order 2-Me-THF > CH_2Cl_2 > CH_3CN. Further, concentration dependant PL experiment was carried out in 2-Me-THF at two different concentrations (10^{-5} and 10^{-7} M) which showed insignificant LE emission (dual emission) at 10^{-7} M relative to that for 10^{-5} M (Fig. S15). In addition, LE band vanished in 10^{-5} M solution in methanol (Fig. S15). The results indicated the formation of dynamic emissive excimer or ICT state in 2-Me-THF most probably via IQ arms. In contrast, H-bonding between the chromophores and MeOH molecules provide a good fixation and

Table 2
Selected EL properties of devices shown in Fig. 10.

EL property	CBP host	no host
η_{max} (%)	0.31	0.04
CIEx	0.281	0.244
CIEy	0.269	0.186

separation for each emitter leading to emission from single, non-excimer molecules. It has also been supported by more red-shifted emission of HE band in MeOH compared to that in 2-Me-THF, which may be due to reorganization of the fluorophores via H-bonding with solvent molecules. Furthermore, in 2-Me-THF two short decay components (lifetimes $\tau_1 = 1.4$ and $\tau_2 = 5.0$ ns) and in MeOH a single component ($\tau = 8.7$ ns) has been detected (Fig. S15, SI) at 407 and 422 nm. Typical single decay behavior is characteristic for undisturbed fluorescence, while two decay components mean two different kinetic processes originating from a single molecule and an excimer or ICT state. Indeed, a brighter PL in MeOH compared to that in 2-Me-THF under UV lamp have been observed by naked eye and shorter decay components in 2-Me-THF indicate a quenching process in 2-Me-THF.

3.4.3. Excimer or ICT induced emission

Dynamic states of excimer or ICT may hamper the OLED construction and therefore use of additional host layers is required that add to complexity and costs of device fabrication. Although, **1** and **2** displayed weaker PL signals via the formation of excimer or ICT states compared to single-decay emission observed in MeOH. Surprisingly, in solid state these showed an overall increase in emission intensity. Emission spectra of **1** and **2** in powdered form also displayed two emission bands, weak emission at 410 (**1**), 415 nm (**2**) and strong PL at 522 (**1**), 529 nm (**2**) contrary to that observed in 2-Me-THF (Fig. 6). This conflicting trend may plausibly be ascribed to the better excimer formation or ICT state in the solid state.

It is evident that HE emission band is due to single molecular emission while low energy band characteristic requires a better insight. The vigilant observation on the reverse trend of dual emissions in solution and solid state led us to come up with the most plausible explanation (Figs. 5 and 6). In the solid state, molecules **1** or **2** are mostly disposed in a fashion to form emissive excimers or ICT states via planar Imidazo-quinazoline (IQ) fluorophore thereby increasing the PL intensity of LE band whereas HE band emits weakly. In contrast, in solution state, **1** or **2** mostly behave as single molecules to exhibit single molecular emission and rather smaller amount of excimers or ICT states thereby

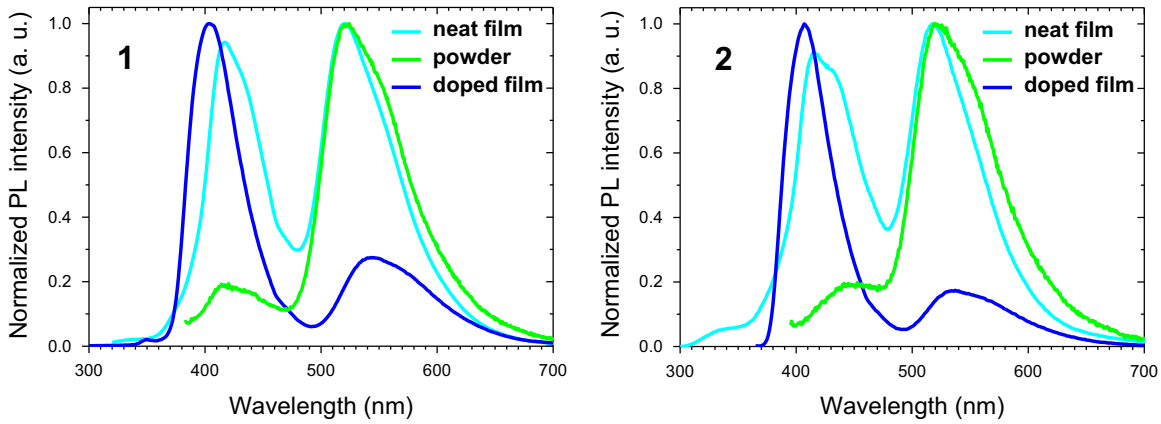

Fig. 6. PL spectra of 1 (left) and 2 (right) in mCP film, 4 and 5 wt%, respectively (blue line), powder (green line), and non-doped neat film (cyan line). (For interpretation of the references to color in this figure legend, the reader is referred to the web version of this article.)

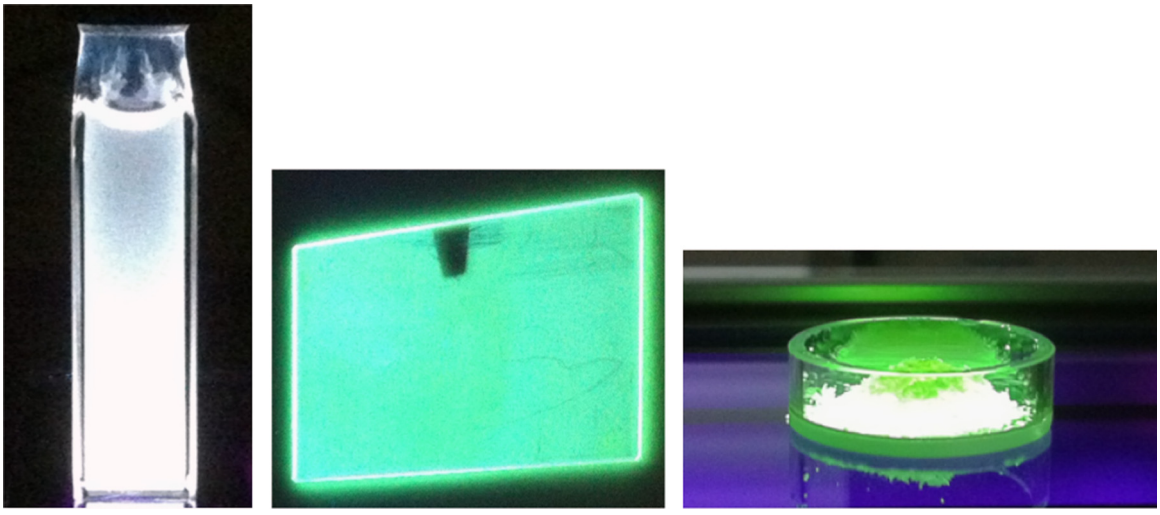

Fig. 7. PL photographs of 1 or 2 dissolved in 2-Me-THF (left), as vacuum-deposited non-doped neat films (center), and in powder state (right) (For interpretation of the references to color in this figure, the reader is referred to the web version of this article.)

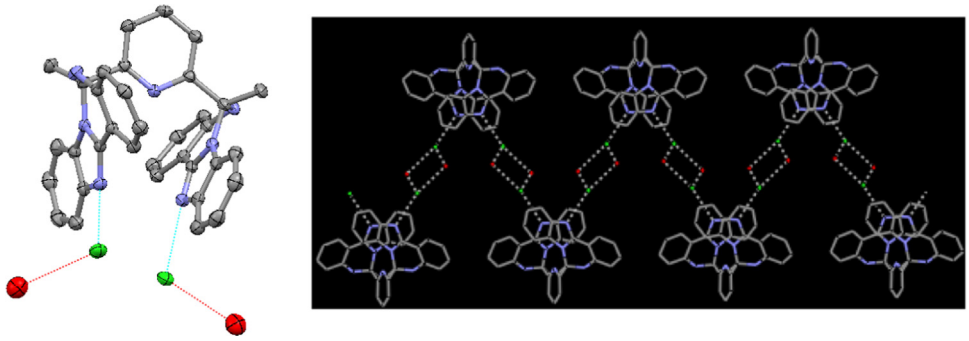

Fig. 8. Crystal structure of model compound M (left); molecular arrangement of M interacting through H · · · bonding (right).

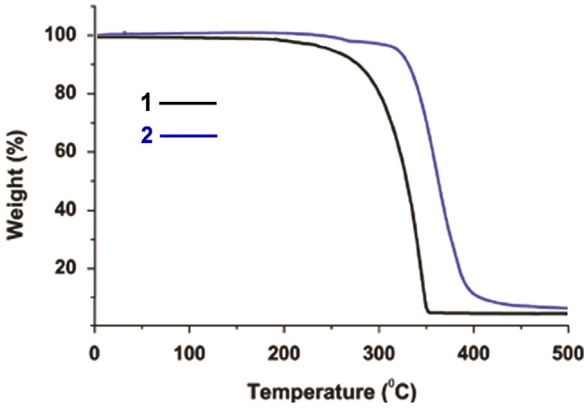

Fig. 9. TGA plots for 1 and 2 in the range 0–500 °C.

increasing the PL intensity of HE band whereas LE band becomes weakly intense. However, formation of emissive excimers or ICT states prefers aprotic non-polar solvents like 2-me-THF but not protic polar solvents like MeOH.

Notably, PL for **1** and **2** in high vacuum-deposited non-doped (neat) films exhibited LE and HE bands of almost equal intensities in the same region (417 and 521 nm, **1**; 410 and 528 nm,**2**), shown in Fig. 6. This emission pattern suggests almost equal contribution of single molecular emission and excimer/ICT in non-doped neat film relative to powdered form. Therefore, emission from single and excimer molecules contribute virtually equally in non-doped neat film. Further, emission behavior of **1** and **2** in host film 1,3-bis (9-carbazolyl)benzene **(mCP)** (4 and 5 wt%, respectively) resembles to that observed in 2-Me-THF (Figs. 5 and 6). Lower contribution of the LE band may be attributed to destruction of excimer/ICT states upon deposition to mCP film. A similar effect, *i.e.* decrease in intensity of the LE (green) emission for powdered **1** or **2** upon grinding has been observed by naked eye under UV lamp exposure. Thus, different degree of excimer/ICT state formation in **1** or **2** results in diverse PL colors, as shown in Fig. 7.

The highest Φ_{PL} was found for **1** in powder form, which is in agreement with greater extent of intermolecular interactions relative to **2**. The values of Φ_{PL} for **1** and **2** in powder, neat film, and mCP are 42.6, 33.3, and 28.4% for **1** and 22.2, 26.5, and 24.0% for **2** (Tables 1) [44–47]. Thus, relatively high Φ_{PL} for **1** may be ascribed to pronounced excimer formation over the **c**ross arrangement of IQ arms in **2** (Fig. S11, SI).

3.5. Development and studies of model compound (M)

Considering the mutually perpendicular orientation of IQ fluorophore arms in **2** (Fig. 2, dimer) we tried to prepare a complex based on it having both the IQ fluorophore arms co-planar. Surprisingly, treatment of **2** with $FeCl_3$ led to a product lacking metal center iron in its structure rather both the IQ fluorophores having parallel orientation with respect to each other (Fig. 8) [41]. Moreover, two molecules each of H_2O and HCl occupy the crystal lattice through intermolecular hydrogen bonding. The conformational switching of IQ fluorophore arms along with intermolecular H · · · bonding with lattice H_2O and HCl enable this product to act as a model compound (**M**) as far as photophysical properties are concerned. Interestingly, chromogenic, fluorogenic and thermal properties of **M** changes significantly relative to **1** and **2** [41]. The model compound does not show any dual emission specially a LE band around 534 nm as in the case of **2**. This significant difference in photophysical behavior of **M** to that of **1** or **2** may be attributed to enhanced hydrogen bonding interactions due to presence of H_2O and HCl (Fig. 8). These weak interactions basically influence the excimer/ICT state formation thus brings down the chances of dual emission in **M** (Fig. 8, right).

3.6. Thermal analysis

Dual emissive compounds with broad features could find application as WOLEDs therefore measurement of thermal properties of emitters becomes essential. Thermogravimetric analysis (TGA) of **1** and **2** showed that former is stable to 254 °C while latter up to 272 °C. Further, these exhibit sharp weight loss of 75.0% (**1**) and 85.9% (**2**) due to loss of IQ units from respective molecules (Fig. 9). Analogous TGA plot for **1** and **2** clearly suggested almost insignificant effect of the number of IQ units on their thermal behavior.

3.7. OLED behavior of 1 and 2

To reproduce emission bands having nearly the same intensity in non-doped neat **1** and **2** under electrical injection, high-vacuum deposited multi-layer OLEDs were fabricated using these compounds as emitting layer (EML). We employed a proven device structure with good charge carrier balance [48], and replaced its EML with a non-doped neat or doped layer **of 1**/**2** : indium tin oxide (ITO; 110 nm)/N, N′-bis(naphthalen-1-yl)-N,N'-bis(phenyl)-2,2′-dimethylbenzidine (α-NPD; 35 nm)/**1**or **2**/4,4′-bis(carbazol-9-yl)-biphenyl (CBP; 15 nm)/ 1,3,5-tris(N-phenylbenz-imidazole-2-yl)benzene (TPBI; 65 nm)/ lithium-fluoride (LiF; 0.8 nm)/aluminum (Al; 70 nm). Here, α-NPD and TPBI served as the hole- and electron transport layers (HTL, ETL), respectively, ITO was the anode, and LiF the electron injecting layer. The HOMO-LUMO energy diagrams for these devices are depicted in Fig. S16. Devices based on both **1** and **2** as EML displayed two emission bands, a HE band with high intensity and LE band with very low (non-doped film) and low (doped) intensities, respectively (Fig. 10). The 1931 Commission Internationale de l'Eclairage (CIE) color coordinates and the maximum EL efficiencies (external quantum efficiencies, η_{max}) of the devices with and without CBP host are listed in Table 2. The HE and LE bands appeared at same position

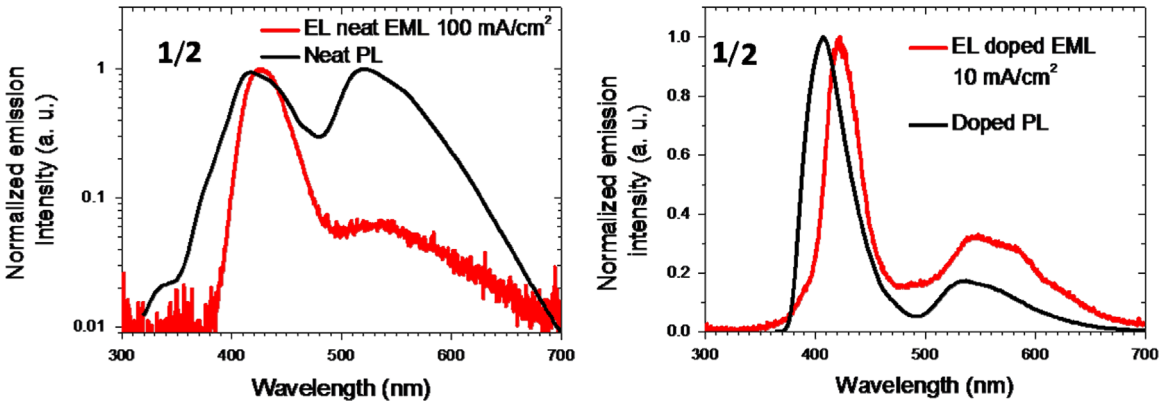

Fig. 10. EL and PL spectra of OLEDs of 1 or 2 based on non-doped (left) and doped (right) emitting layers.

compared to PL spectra of the non-doped or doped films except for rather red shifted HE EL band for the doped film (Fig. 10). The latter difference may originate in different host materials. Besides, fluorescence from the assisting layers (α-NPD, CBP, and TPBI) would be in other spectral regions compared to the one observed in EL spectra, thus two emission bands originate from **1** or **2**. On the other hand, lack of emission bands with nearly same intensities in devices with single EML suggested destruction of the excimer/ICT state under electrical injection. This unusual observation is in contrary to other reports [49–51], and probably related to electrical stability of **1** and **2**, further discussed in the next session. Thus, two-band emissions with same intensities in devices containing neat **1** or **2** could not be achieved (Fig. 10).

It is interesting to note that a rapid decrease in EL occurred for the OLEDs fabricated using **1** or **2** as emitters. The EL signal was coupled to a spectrometer via an optical fiber and monitored over the scale of several to tens of seconds at a constant voltage and current. Intensity of the EL spectrum rapidly decreased below 50% of its original value in about 30 s (Fig. S17). Further, intensity of HE band diminished much more swiftly than LE band for the devices with doped **1**or **2** EML layer. We suspect that weak electrical stability of devices based on **1** and **2** as EMLs is caused by free –N*H* groups present in these compounds, therefore should be avoided in EL applications [52,53]. For better understanding of this effect, future analyses could involve design of OLEDs lacking direct carrier injection into emitting material containing free –N*H* groups. This approach is expected to prevent degradation of EL, but would inevitably require the use of host layers.

4. Conclusion

Through this work, we have described design and synthesis of mono- and dimeric quinazoline derivatives **1** and **2**. Comparative photophysical properties of these compounds in 2-Me-THF, powder, non-doped (neat), and deposited in host films, clearly suggested insignificant influence of the number of appended fluorophore units in mono-/dimer, unless there is an extended conjugation between central unit and fluorophores. This conclusion has further been strongly supported by theoretical calculations and thermal analysis. Further, **1** and **2** display broad emission features of two bands with nearly equal intensity stretching through a wide range of visible spectrum in neat films, thanks to a co-existing high and low energy (LE) emission band. The LE band originates from dynamic excimer or ICT state formation. Unfortunately, nearly equal-intensity emission bands could not be reproduced under electrical injection. In addition, both **1** and **2** showed rapid OLED device degradation under electrical current flow ascribed to the presence of free –N*H* groups.

Acknowledgments

Authors acknowledge the Department of Science and Technology (DST), New Delhi, India for providing financial assistance through the scheme SR/S1/IC/-25/2011 (DSP) and DST Inspire Faculty Scheme (IFA12-CH-66) to RP. This research is supported by the Cabinet Office, Government of Japan and the Japan Society for the Promotion of Science (JSPS) through the Funding Program for World-Leading Innovative R&D on Science and Technology (FIRST Program). The authors thank Dr. K. Goushi for helpful suggestions and discussions.

Appendix A. Supporting information

Supplementary data associated with this article can be found in the online version at http://dx.doi.org/10.1016/j.jlumin.2016.09.026.

References

[1] J. Roncali, Chem. Rev. 97 (1997) 173.
[2] N.S. Sariciftci, L. Smilowitz, A.J. Heeger, F. Wudl, Science 258 (1992) 1474.
[3] R. Bergera, A.L. Domanskia, S.A.L. Weber, Eur. Polym. J. 49 (2013) 1907.
[4] W.C.H. Choy, W.K. Chan, Y. Yuan, Adv. Mater. 26 (2014) 5368.
[5] W. Hu, Z. Bao, K. Muellen, J. Mater. Chem. 22 (2012) 4134.
[6] F. Garnier, R. Hajlaoui, A. Yassar, P. Srivastava, Science 265 (1994) 1684.
[7] C.W. Tang, S.A. VanSlyke, Appl. Phys. Lett. 51 (1987) 913.
[8] C.W. Tang, S.A. VanSlyke, C.H. Chen, J. Appl. Phys. 65 (1989) 3610.
[9] F. Garnier, Acc. Chem. Res. 32 (1999) 209.
[10] Y. Sagara, T. Mutai, I. Yoshikawa, K. Araki, J. Am. Chem. Soc. 129 (2007) 1520.
[11] S.J. Yoon, J.W. Chung, J. Gierschner, K.S. Kim, M.G. Choi, D. Kim, S.Y. Park, J. Am. Chem. Soc. 132 (2010) 13675.
[12] D.G. Wu, C.H. Huang, L.B. Gan, W. Zhang, J. Zheng, H.X. Luo, N.Q. Li, J. Phys. Chem. B 103 (1999) 4377.
[13] D.G. Wu, C.H. Huang, Y. Huang, L.B. Gan, A.C. Yu, L.M. Ying, X.S. Zhao, J. Phys. Chem. B 103 (1999) 7130.
[14] F.Y. Li, J. Zheng, C.H. Huang, L. Jin, Y. Haung, J. Gao, T. Liu, X. Zhao, Appl. Surf. Sci. 161 (2000) 178 and references therein.
[15] G.J. Ashwell, P.D. Jackson, W.A. Crossland, Nature 368 (1994) 438.
[16] Z.S. Wang, F.Y. Li, C.H. Huang, L. Wang, M. Wei, L.P. Jin, N.Q. Li, J. Phys. Chem. B 104 (2000) 9676.
[17] X. Song, J. Perlstein, D.G. Whitten, J. Am. Chem. Soc. 117 (1995) 7816.
[18] S. Zeena, K.G. Thomas, J. Am. Chem. Soc. 123 (2001) 7859.
[19] G.P. Bartholomew, G.C. Bazan, Acc. Chem. Res. 34 (2001) 30.
[20] R.W. Chambers, T. Kajiwara, D.R. Kearns, J. Phys. Chem. 78 (1974) 380.
[21] Y. Huang, T. Cheng, F. Li, C.-H. Huang, J. Phys. Chem. B 106 (2002) 10020.
[22] T.G. Goodson, Acc. Chem. Res. 38 (2005) 99.
[23] C. Katan, F. Terenziani, O. Mongin, M.H.V. Werts, L. Porres, T. Pons, J. Mertz, S. Tretiak, M. Blanchard-Desce, J. Phys. Chem. A 109 (2005) 3024.
[24] J.C. Kirkwood, C. Scheurer, V. Chernyak, S. Mukamel, J. Chem. Phys. 114 (2001) 2419.
[25] J.H. Burroughes, D.D.C. Bradley, A.R. Brown, R.N. Marks, K. Mackay, R.H. Friend, P.L. Burns, A.B. Holms, Nature 347 (1990) 539.
[26] H. Aziz, Z.D. Popovic, N.-X. Hu, A.-M. Hor, G. Xu, Science 283 (1999) 1900.
[27] Y.Z. Wu, X.Y. Zheng, W.Q. Zhu, R.G. Sun, X.Y. Jiang, Z.L. Zhang, S.H. Xu, Appl. Phys. Lett. 83 (2003) 5077.

[28] S.W. Culligan, A.C.-A. Chen, J.U. Wallace, K.P. Klubek, C.W. Tang, S.H. Chen, Adv. Funct. Mater. 16 (2006) 1481.
[29] S.Y. Ni, X.R. Wang, Y.Z. Wu, H.Y. Chen, W.Q. Zhu, X.Y. Jiang, Z.L. Zhang, Appl. Phys. Lett. 85 (2004) 6.
[30] A.K. Agrawal, S.A. Jenekhe, Chem. Mater. 8 (1996) 579.
[31] S. Tao, L. Li, J. Yu, Y. Jiang, Y. Zhou, C.-S. Lee, et al., Chem. Mater. 21 (2009) 1284.
[32] Z. Wang, P. Lu, S. Chen, Z. Gao, F. Shen, W. Zhang, et al., J. Mater. Chem. 21 (2011) 5451.
[33] H. Huang, X. Yang, B. Pan, L. Wang, J. Chen, D. Ma, et al., J. Mater. Chem. 22 (2012) 13223.
[34] X. Yang, S. Zheng, R. Bottger, H.S. Chae, T. Tanaka, S. Li, et al., J. Phys. Chem. C 115 (2011) 14347.
[35] S. Park, J.E. Kwon, S.H. Kim, J. Seo, K. Chung, S.-Y. Park, et al., J. Am. Chem. Soc. 131 (2009) 14043.
[36] G.M. Farinola, R. Ragni, Chem. Soc. Rev. 40 (2011) 3467.
[37] S. Mukherjee, P. Thilagar, Dyes Pigment. 110 (2014) 2.
[38] D.D. Perrin, W.L.F. Armango, D.R. Perrin, Purification of Laboratory Chemicals, Pergamon, Oxford, U.K, 1986.
[39] (a) G.M. Sheldrick, SHELXL-97, Program for X-ray Crystal Structure Refinement, Gottingen University, Gottingen, Germany, 1997;
(b) G.M. Sheldrick, SHELXS-97, Program for X-ray Crystal Structure Solution, Gottingen University, Gottingen, Germany, 1997.
[40] (a) A.L. Spek, PLATON, A Multipurpose Crystallographic Tools, Utrecht University, Utrecht, The Netherlands, 2000;
(b) A.L. Spek, Acta Crystallogr. A 46 (1990) C31.
[41] R. Pandey, G. Méhes, A. Kumar, R.K. Gupta, C. Adachi, D.S. Pandey, Chem. Commun. 50 (2014) 8032.
[42] R. Pandey, M. Yadav, M. Shahid, A. Misra, D.S. Pandey, Tetrahedron Lett. 53 (2012) 3550.
[43] R. Pandey, R.K. Gupta, M. Shahid, B. Maiti, A. Misra, D.S. Pandey, Inorg. Chem. 51 (2012) 298.
[44] K. Suzuki, Nat. Photonics (2011) ***5***.
[45] R. Karpicz, S. Puzinas, S. Krotkus, K. Kazlauskas, S. Jursenas, J.V. Grazulevicius, S. Grigalevicius, V. Gulbinas, J. Chem. Phys. 134 (2011) 204508.
[46] E. Turner, N. Bakken, J. Li, Inorg. Chem. 52 (2013) 7344.
[47] S. Ghosh, A.K. Mitra, C. Saha, S. Basu, J. Fluoresc. 23 (2013) 1179.
[48] H. Uoyama, K. Goushi, K. Shizu, H. Nomura, C. Adachi, Nature 492 (2012) 234.
[49] W.-L. Gong, B. Wang, M.P. Aldred, C. Li, G.-F. Zhang, T. Chen, L. Wang, M.-Q. Zhu, J. Mater. Chem. C 2 (2014) 7001.
[50] Y. Gong, J. Liu, Y. Zhang, G. He, Y. Lu, W.B. Fan, W.Z. Yuan, J.Z. Sun, Y. Zhang, J. Mater. Chem. C 2 (2014) 7552.
[51] L. Chen, Y. Jiang, H. Nie, P. Lu, H.H.Y. Sung, I.D. Williams, H.S. Kwok, F. Huang, A. Qin, Z. Zhao, B.Z. Tang, Adv. Funct. Mater. 24 (2014) 3621.
[52] H. Yersin, A.F. Rausch, R. Czerwieniec, T. Hofbeck, T. Fischer, Coord. Chem. Rev. 255 (2011) 2622.
[53] T. Sajoto, P.I. Djurovich, A.B. Tamayo, J. Oxgaard, W.A. Goddard, M.E. Thompson, J. Am. Chem. Soc. 131 (2009) 9813.